



Original Article

Longitudinal subcortical volume changes and their correlations with multiple PET and fluid biomarkers in dominantly inherited Alzheimer's disease

IL Han Choo^{a,b,*}, Hoyoung Park^c, Brian A. Gordon^d, Randall J. Bateman^d, the Dominantly Inherited Alzheimer Network^{#,^}

^a Chosun University, College of Medicine, Department of Neuropsychiatry, Gwangju, South Korea

^b Karolinska Institutet, Center for Alzheimer Research, Division of Clinical Geriatrics, Stockholm, Sweden

^c Sookmyung Women's University, Research Institute of Natural Science, Department of Statistics, Seoul, South Korea

^d Washington University School of Medicine, St Louis, MO, USA



ARTICLE INFO

Keywords:

Longitudinal

Subcortical volume

Dominantly inherited Alzheimer's disease

Biomarkers correlations

ABSTRACT

Background: Alzheimer's disease postmortem studies demonstrate that amyloid plaques and neurofibrillary tangles are present in subcortical regions.

Objective: To investigate longitudinal subcortical structural changes in autosomal dominant Alzheimer's disease in relation to multiple PET and fluid biomarkers.

Design: Dominantly Inherited Alzheimer's Network (DIAN) Observational study

Setting: Multicenter study

Participants: Participants were identified as mutation-carriers of pathologic variants in presenilin-1, presenilin-2, or amyloid precursor protein and as non-carriers from the same families as the mutation-carriers. They underwent baseline and 2 and more times longitudinal follow-up assessments of multiple biomarkers

Measurements: Participants underwent structural MRI, ¹¹C-Pittsburgh Compound B PET, ¹⁸F-fluorodeoxyglucose PET, and CSF and plasma assessments. Rates of biomarker change as a function of estimated years to symptom onset were estimated using multivariate linear mixed-effects models, and longitudinal associations between subcortical atrophy and multiple biomarkers were evaluated.

Results: A total of 601 participants completed one or more clinical evaluations, with up to eight annual visits. Mutation carriers showed significantly greater longitudinal atrophy in the left amygdala, bilateral thalamus, putamen, nucleus accumbens, and hippocampus compared with non-carriers (Bonferroni-corrected $p < 0.05$). The earliest divergence was observed 13.2 years before the expected symptom onset in the right nucleus accumbens, following amyloid- β ($A\beta$) accumulation in the right thalamus that began 23.8 years before onset. Among carriers, atrophy in the right thalamus, bilateral putamen, and bilateral nucleus accumbens was significantly associated with region-specific or cortical $A\beta$ accumulation, as well as with CSF $A\beta_{42}$, $A\beta_{42}/A\beta_{40}$ ratio, total tau, and phosphorylated tau (Bonferroni-corrected $p < 0.05$).

Conclusions: The present findings may provide a unique and well-characterized model for investigating the temporal ordering of Alzheimer's disease biomarkers.

1. Introduction

Alzheimer's disease dementia (AD) is most common cause of dementia worldwide. Studies of individuals from families with autosomal

dominant Alzheimer's disease (ADAD) provide a unique opportunity to characterize the earliest pathophysiological changes that occur before symptom onset. While magnetic resonance imaging (MRI) investigations in AD have primarily focused on the cerebral cortex and reported only

* Corresponding author at: Chosun University, College of Medicine, Gwangju, South Korea

E-mail address: ilhan.choo@chosun.ac.kr (I.H. Choo).

[#] For more on the DIAN observational study see <http://www.dian-info.org>.

[^] Additional details are available in the attached file titled "DIAN Consortium Author List_2024.xls".

cross-sectional findings, [1,2] postmortem studies demonstrate that amyloid plaques and neurofibrillary tangles are also present in subcortical regions [3,4] Consistently, amyloid positron emission tomography (PET) studies in presymptomatic familial AD have identified the striatum and thalamus as early sites of amyloid deposition, [5] and reductions in subcortical volume have been associated with both clinical severity and cognitive decline [6]

Findings from the Dominantly Inherited Alzheimer Network (DIAN) further highlight the importance of these regions: significant gray matter volume differences between noncarriers and mildly symptomatic carriers (Clinical Dementia Rating [CDR] 0.5) have been observed in the thalamus and putamen [7] However, subsequent longitudinal DIAN studies have not focused on the difference in rate of subcortical volume change between carriers and non-carriers [8,9] This gap in knowledge is clinically relevant, as MRI—widely used in routine diagnostic practice—could provide a cost- and time-efficient means to detect such changes. If MRI-based measures of subcortical atrophy can be incorporated into early diagnostic strategies, analogous to plasma phospho-tau217, [10] they could facilitate broader population screening than methods based on PET or cerebrospinal fluid (CSF) analysis.

To date, no study has comprehensively investigated longitudinal subcortical structural changes in ADAD in relation to multiple PET and fluid biomarkers. We therefore hypothesized that (1) the rates of a priori-selected subcortical regional atrophy differ longitudinally, relative to estimated years to symptom onset, between mutation carriers and non-carriers; and (2) subcortical regions showing significant longitudinal differences by mutation status also demonstrate longitudinal associations with amyloid burden (¹¹C-Pittsburgh compound B [PIB] PET), glucose metabolism (¹⁸F-fluorodeoxyglucose [FDG] PET), and fluid biomarkers (CSF Aβ42, Aβ42/Aβ40, CSF Tau, CSF pTau, Plasma Aβ1-42, Plasma Aβ1-42/Aβ1-40).

2. Methods

2.1. Study design and participants

Individuals were included from the DIAN Observational Study (the 16th semiannual data freeze). Participants were identified as mutation-carriers (MCs) of pathologic variants in presenilin-1 (PSEN1), presenilin-2 (PSEN2), or amyloid precursor protein (APP) and as non-carriers (NCs) from the same families as the MCs. They underwent baseline and 2 and more times longitudinal follow-up assessments of PIB/FDG-PET, MRI, CSF Aβ42, CSF Aβ40, CSF Tau, CSF pTau, Plasma Aβ1-42, Plasma Aβ1-40.

DIAN estimated years to symptom onset (EYO) was calculated for symptomatic individuals with reported decline ages, their EYO = visit age – the mean of decline ages and for asymptomatic individuals, their EYO = their mutation/parental EYO.

Cognitive status was determined using the Clinical Dementia Rating (CDR) scale [11] Non-carriers (NCs) with a CDR of 0 were classified as cognitively normal (NC_CN). Mutation carriers (MCs) with CDR = 0 were classified as presymptomatic (MC_p), whereas participants with CDR > 0 were considered symptomatic. Participants with CDR = 0.5 were classified as having mild cognitive impairment (MCI) and were categorized as NCs with MCI (NC_MCI) or MCs with MCI (MC_MCI) based on mutation status. Mutation carriers meeting clinical criteria for Alzheimer's disease were classified as MC_AD, including individuals with CDR = 0.5 or greater. NC_MCI participants represent mutation non-carriers from DIAN families and do not reflect sporadic Alzheimer's disease. Apolipoprotein E (APOE) ε4 status was dichotomized as ε4 carriers (E4+, including heterozygotes and homozygotes) or ε4 non-carriers (E4–) (Table 1).

DIAN participants provided informed consent in accordance with the local institutional review boards of each participating site. DIAN study procedures have received ethics approval by the Human Research Protection Office at Washington University in St. Louis (MO, USA) and all of the participating sites. Additional institutional review board approval (CHOSUN 2024-08-019-002) was received from Chosun University Hospital for data analysis.

Table 1
Demography and Clinical Information.

	NC_CN (n = 221)	NC_MCI (n = 16)	MC_p (n = 236)	MC_MCI (n = 64)	MC_AD (n = 64)
Age, Mean (SD)	37.49 (11.04)	40.68 (13.03)	34.20 (9.16)	42.94 (10.12)	48.81 (8.97)
Female %	58.82	56.25	58.05	59.38	43.75
Estimated years of symptom onset, Mean (SD)	48.76 (6.33)	48.41 (4.77)	48.51 (6.81)	45.54 (6.39)	45.16 (7.97)
CDR, Mean (SD)	0.00 (0.00)	0.47 (0.12)	0.01 (0.10)	0.49 (0.11)	1.13 (0.73)
Family mutation PSEN1/PSEN2/APP (%)	70/10/20	56/0/44	70/11/19	80/<5/19	84/2/14
APOE E4+ (number, %)	69 (31.22%)	5 (31.25%)	70 (29.56%)	17 (26.56%)	19 (29.69%)
APOE E4- (number, %)	152 (68.78%)	11 (68.75%)	166 (70.34%)	47 (73.44%)	45 (70.31%)
Visit distribution	{1: 78, 2: 64, 3: 39, 4: 23, 5: 20, 6: 5}	{1: 13, 3: 4, 4: 1}	{1: 76, 2: 83, 3: 36, 4: 23, 5: 18, 6: 4, 8: 1}	{1: 32, 2: 26, 3: 8, 4: 6, 6: 1}	{1: 20, 2: 34, 3: 14, 4: 6, 6: 2}
Follow up Diagnostic Change	NC → NC_MCI: 4 NC → NC_MCI → NC: <5	NC_MCI → NC: 7 NC_MCI → NC → NC_MCI: <5	MC_p → MC_MCI: 14 MC_p → MC_MCI → MC_p: 3 MC_p → MC_MCI → MC_AD: 5 MC_p → MC_AD: <5	MC_MCI → MC_AD: 21 MC_MCI → MC_p: 6 MC_MCI → MC_p → MC_MCI: <5 MC_MCI → MC_p → MC_MCI → MC_AD: <5 MC_MCI → MC_p → MC_AD: <5	MC_AD → MC_MCI: <5

Each Diagnostic group and number were categorized by baseline visit.

NC_CN = mutation non-carriers with cognitively normal; NC_MCI = mutation non-carriers with mild cognitive impairment; MC_p = mutation carriers with pre-symptomatic; MC_MCI = mutation carriers with mild cognitive impairment; MC_AD = Mutation carriers with Alzheimer's disease

Clinical groupings were based on mutation status and clinical criteria. NC_MCI denotes mutation non-carriers from DIAN families with CDR = 0.5 at one or more visits and does not represent sporadic

Alzheimer's disease. MC_AD denotes mutation carriers meeting clinical criteria for Alzheimer's disease and may include individuals with CDR = 0.5 or greater. APOE ε4 carrier status is indicated as E4+(heterozygous or homozygous) or E4–. Visit distribution was displayed by visit count: distinct numbers of ID. These distinct ID numbers were also used in follow up diagnostic change counts.

2.2. MRI Imaging and Processing

Structural MRI acquisition was performed using the Alzheimer Disease Neuroimaging Initiative (ADNI) protocol [12,13]. Participating sites were required to pass initial and regular follow-up quality control assessments to insure acquisition conformity. Each participant received an accelerated 3D sagittal T1-weighted MPRAGE on a 3T scanner. A high quality, whole-brain image with $1.1 \times 1.1 \times 1.2$ mm voxels was acquired in approximately 5-6 minutes. Before analysis, images were screened for artifacts and protocol compliance by the ADNI imaging core. FreeSurfer analysis involves subcortical reconstruction and volumetric segmentation of T1 weighted images [14]. MRI regional volumes were corrected for head size (intracranial volume, ICV) in order to have correct comparisons as follows: First, Compute mean ICV for sample; Second, Compute regression with ICV as independent variable and an ROI as dependent variable to obtain B weight; Third, Compute: Normalized = raw volume - (B-weight * (ss ICV - mean ICV)) ("ss" = single subject's).

2.3. PET Processing

Each site underwent an initial evaluation by the ADNI PET QC site to ensure compliance with a common PIB, FDG PET protocol. Amyloid imaging was performed with a bolus injection of approximately 15 mCi of PIB. Dynamic imaging acquisition started either at injection for 70 minutes or 40 minutes post-injection for 30 minutes. For analysis, the PIB PET data between 40 to 70 minutes was converted to regional standardized uptake value ratios (SUVRs). Metabolic imaging with FDG-PET was performed with a 3D dynamic acquisition began 40 minutes after a bolus injection of approximately 5 mCi of FDG. Data from the last 20 minute of each FDG scan were converted to SUVRs relative to cerebellar grey matter. PET imaging analyses are performed using the PET unified pipeline [15,16]. PET images are smoothed to achieve a common spatial resolution of 8mm to minimize inter-scanner differences [17]. Inter-frame motion correction for the dynamic PET images is performed using standard image registration techniques [18,19]. PET-MR registration is performed using a vector-gradient algorithm (VGM)[20] in a symmetric fashion (i.e. average transformation for PET->MR and inverse of MR->PET was used as the final transformation matrix). By default, regional PET processing is performed based on FreeSurfer segmentation (using wmparc.mgz as the region definition), and each FreeSurfer region is analyzed. To assess global amyloid burden based on amyloid PET imaging data, the arithmetic mean SUVR from precuneus, prefrontal cortex, gyrus rectus, and lateral temporal regions are defined as the mean cortical SUVR.

2.4. Biofluids Analysis

Protocols for the collection of cerebrospinal fluid (CSF) and blood (for plasma) are consistent with the biofluid protocol of the Alzheimer's Disease Neuroimaging Initiative (ADNI) (<http://www.adni-info.org/>). CSF amyloid β 42 (A β 42), tau (Tau), and phosphorylated tau-181 (pTau) were measured by immunoassay using Luminex bead-based multiplexed xMAP technology (INNO-BIA AlzBio3, Innogenetics). Concentrations of CSF A β 40 were measured by plate-based enzyme-link immunosorbent assay (ELISA) (research prototype INNOTEST™

A β 40, Innogenetics, Ghent, Belgium). A β 42 estimates were normalized for individual differences in CSF production rates by forming a ratio with A β 40 as the denominator [21]. Blood samples were collected via venipuncture under fasting conditions. Concentrations of plasma A β species (A β 1-40, A β 1-42) were measured by xMAP (INNO-BIA Plasma A β Forms Multiplex Assay™, Innogenetics, Ghent, Belgium) [22].

2.5. Statistical analysis

All statistical analyses were performed using R version 4.5.0 (The R

Foundation for Statistical Computing, <http://www.r-project.org/>). A two-step analytical framework was employed to test our hypotheses.

In the first step, we conducted reference analyses using multivariate linear mixed-effects models (LMMs) implemented via the lme4 (version 1.1-35.3) and lmerTest (version 3.1-3) packages. The models included fixed effects for estimated years from symptom onset (EYO), mutation status (autosomal dominant Alzheimer's disease (ADAD) mutation carriers vs. non-carriers), and time from baseline, along with all possible two-way and three-way interaction terms. Sex, years of education, and APOE ϵ 4 carrier status were considered as additional covariates. Each covariate was individually added to the baseline model—which already included all fixed effects and interaction terms—and evaluated using a likelihood ratio test via ANOVA. Only covariates that showed a statistically significant improvement in model fit ($p < 0.05$) were retained in the final model specification. The random effects included in the models were the random intercepts for family clusters, individual random intercept and random slope with a *diagonal* covariance matrix, to account for the within-subject correlation due to repeated measures. These models were applied to examine the differential longitudinal trajectories of established AD biomarkers, including PIB and FDG PET measures, CSF A β 42, CSF A β 42/A β 40 ratio, CSF Tau, CSF pTau, plasma A β 1-42, and plasma A β 1-42/A β 1-40 ratio. In parallel, we examined longitudinal subcortical volume changes using the same LMM specification. Seven subcortical regions of interest (ROIs) — the amygdala, putamen, thalamus, caudate, pallidum, nucleus accumbens, and hippocampus — were each analyzed bilaterally, yielding a total of 14 ROI assessments based on a priori laterality hypotheses.

Laterality was explicitly prespecified rather than inferred post hoc. Left and right hemisphere ROIs were modeled independently in all longitudinal analyses, without averaging across hemispheres, to capture potential asymmetries in disease-related atrophy trajectories. Statistical significance was determined based on Bonferroni-adjusted p-values with a significance threshold of 0.05. For all significant findings, we further identified the specific EYO points at which significant group-level differences between mutation carriers and non-carriers began to emerge. Our primary statistical inference was based on the linear mixed-effects model estimates. For visualization purposes, locally estimated scatterplot smoothing (LOESS) was applied separately to mutation carriers and non-carriers to illustrate potential nonlinear trends in longitudinal trajectories. Importantly, all primary statistical inferences were based on the linear mixed-effects models. Divergence points were operationally defined as the earliest estimated year at which the 99% confidence intervals of the LOESS-predicted trajectories for mutation carriers and non-carriers no longer overlapped, and only in cases where a statistically significant interaction between estimated years to symptom onset and mutation status was identified in the corresponding mixed-effects model. This approach ensured consistency between inferential statistics and graphical visualization while providing an intuitive representation of group-level divergence over time.

In the second step, we explored whether the subcortical regions that showed significant longitudinal differences by mutation status in the first-step analysis were also longitudinally associated with the aforementioned AD biomarkers. Specifically, we assessed whether subcortical volume trajectories were linked to markers of amyloid burden (e.g., PIB SUVR), glucose metabolism (FDG SUVR), CSF A β 42 and A β 42/A β 40, tau pathology (CSF Tau and pTau), and plasma A β species. For these LMM, we calculated the conditional coefficient of determination (R^2_c), which quantifies the variance explained by both fixed and random effects, using the MuMIn package (version 1.47.5). These analyses allowed us to evaluate the extent to which subcortical atrophy was coupled with multiple domains of AD pathology, particularly in mutation carriers.

3. Results

Demographic and clinical information on the participants is presented in Table 1. A total of 601 participants underwent one or more

clinical evaluations with a maximum of eight visits and visit distribution details are provided in Table 1. Among them, 221 individuals were classified non-carriers with cognitive normal (NC_CN), and 236 individuals were presymptomatic mutation carriers (MC_p, CDR = 0) and 144 individuals were symptomatic, consisting of 16 non-carriers with mild cognitive impairment (NC_MCI), 64 mutation carriers with mild cognitive impairment (MC_MCI), and 64 mutation carriers with AD (MC_AD) by a CDR score of 0.5 or higher. For the analyses: MRI subcortical volume data were available for 566 individuals, comprising a total of 1330 observations. ¹¹C-PIB PET and ¹⁸F-FDG PET data were available for 532 individuals, totaling 1130 observations. CSF Aβ42 and CSF Aβ42/Aβ40 ratio data were available for 462 individuals, totaling 844 observations. CSF Tau and CSF pTau data were available for 460 individuals, totaling 832 observations. Plasma Aβ1-42 and plasma Aβ1-42/Aβ1-40 ratio data were available for 517 individuals, comprising 1083 observations. Participants with longitudinal data had a mean 2.5 visits (SD 1.5) and 3.1 years (SD 3.0) of data.

3.1. Longitudinal Association of AD biomarkers with Respect to EYO Between Mutation Carriers and Non-Carriers

Reference AD biomarker analyses revealed that mutation carriers exhibited significantly higher rates of increase compared to non-carriers in mean cortical PIB SUVR, CSF Tau, and CSF pTau, and significantly greater rates of decrease in precuneus FDG SUVR, CSF Aβ42, and CSF Aβ42/Aβ40 ratio. The estimated points of divergence between mutation carriers and non-carriers occurred at 22.5, 19.2, and 21.5 years before expected symptom onset for mean cortical PIB SUVR, CSF Tau, and CSF pTau, respectively, and at 12.0, 13.8, and 17.6 years before expected onset for precuneus FDG SUVR, CSF Aβ42, and CSF Aβ42/Aβ40 (Table 2, Fig. 1). For subcortical regional volumes, 9 out of 14 subcortical ROIs — including the left amygdala, bilateral thalamus, putamen, nucleus accumbens, and hippocampus — demonstrated significant differences between mutation carriers and non-carriers. The earliest divergence was observed in the right nucleus accumbens at 13.2 years before expected symptom onset, with divergence across regions spanning from 13.2 years before to 4.5 years after expected onset (Table 3, Fig. 2). Regarding ¹¹C-PIB PET measures in subcortical regions, 11 out of 14 regions — including the right amygdala, bilateral thalamus, putamen, pallidum, caudate, and nucleus accumbens — showed significantly greater longitudinal rates of amyloid accumulation in mutation carriers relative to non-carriers. The estimated divergence points varied by region, ranging from 23.8 years to 15.7 years before expected symptom onset (Table 4, Fig. 2). In contrast, for ¹⁸F-FDG PET measures, only the left

Table 2
Longitudinal linear mixed-effects model of reference AD biomarkers by estimated years to symptom onset interaction with mutation status.

	Fixed-effects coefficient	SE	df	t-value	p-value
Mean Cortical PIB SUVR	0.022	0.003	280.00	8.19	<0.001*
Precuneus FDG SUVR	-0.008	0.001	305.00	-6.47	<0.001*
CSF Aβ42	-21.087	3.154	252.00	-6.69	<0.001*
CSF Aβ42/Aβ40	-0.001	0.000	250.00	-2.76	0.006*
CSF Tau	3.526	0.585	253.00	6.03	<0.001*
CSF pTau	1.955	0.262	252.00	7.45	<0.001*
Plasma Aβ1-42	-0.023	0.142	540.00	-0.16	0.871
Plasma Aβ1-42/Aβ1-40	0.002	0.001	379.00	1.89	0.060

Mutation status are divided by mutation carriers and non-carriers of autosomal dominant Alzheimer's disease.

* p < 0.05; SE = Standard Error

hippocampus showed a significant decline in FDG SUVR between mutation carriers and non-carriers. Divergence occurred 8.1 years before the expected symptom onset in the left hippocampus (Table 4, Fig. 2).

3.2. Longitudinal Associations Between Defined Subcortical Volumes and AD Biomarkers in Mutation Carriers

The defined subcortical volumes included ten regions of interest (ROIs) — the bilateral amygdala, thalamus, putamen, nucleus accumbens, and hippocampus — which showed significant results in the first-step analyses. The right amygdala was also included due to a significant trend (p < 0.005).

Longitudinal association analyses were conducted exclusively in mutation carriers. Significant longitudinal associations between each subcortical volume and the region-matched PIB SUVR were observed in the bilateral amygdala, right thalamus, bilateral putamen, and bilateral nucleus accumbens (Supplementary Data Table 1, Supplementary Data Fig. 1a). Regarding associations with region-matched FDG SUVR, significant associations were found in the left amygdala, left thalamus, left nucleus accumbens, and bilateral hippocampus (Supplementary Data Table 1, Supplementary Data Fig. 1b). In addition, significantly negative longitudinal associations were identified between mean cortical PIB SUVR and subcortical volumes, except for the left thalamus (Supplementary Data Table 2), whereas significantly positive longitudinal associations were observed between the ten subcortical volumes and precuneus FDG SUVR (Supplementary Data Table 3).

For the analyses examining longitudinal associations between subcortical volumes and fluid AD biomarkers: Significant associations with CSF Aβ42 were found in the left amygdala, right thalamus, bilateral putamen, bilateral nucleus accumbens, and bilateral hippocampus. Significant associations with CSF Aβ42/Aβ40 ratio were observed in the right thalamus, bilateral putamen, bilateral nucleus accumbens, and left hippocampus. Significant associations with CSF Tau were present across all ten defined subcortical ROIs. Significant associations with CSF pTau were found in the left amygdala, right thalamus, bilateral putamen, bilateral nucleus accumbens, and bilateral hippocampus. For plasma biomarkers, significant associations with plasma Aβ1-42 were identified in the right amygdala and right hippocampus, and associations with plasma Aβ1-42/Aβ1-40 ratio were found in the right amygdala, right thalamus, and bilateral hippocampus (Supplementary Data Table 4).

4. Discussion

In the present study, we applied the linear-mixed effects model to reference AD biomarkers, to compare longitudinal trajectories between mutation carriers and non-carriers. Among the biomarkers, mean cortical Aβ deposition was the earliest biomarker to show divergence, with carriers exhibiting significantly greater accumulation beginning 22.5 years before the estimated age of symptom onset. This was followed by divergence in CSF pTau (21.5 years before), CSF Tau (19.2 years), CSF Aβ42/Aβ40 ratios (17.6 years), and CSF Aβ42 (13.8 years). In contrast, precuneus glucose metabolism diverged closer to symptom onset, at 12.0 years prior.

Compared to a previous DIAN longitudinal study, [8] the timepoint of Aβ divergence was similar (22.2 vs. 22.5 years before). However, our finding on glucose metabolism divergence (12.0 years) occurred substantially closer to symptom onset than reported previously (18.8 years). The divergence timepoints for CSF Tau and CSF Aβ42 (19.2 and 13.8 years before onset, respectively) are consistent with prior cross-sectional analyses from the DIAN study (15 and 10 years, respectively), [23] as well as with longitudinal findings from the same cohort, [24] which reported divergence of CSF Tau at 17 years and CSF pTau at 19 years before onset. These prior findings align well with the present results (CSF Tau: 19.2 years; CSF pTau: 21.5 years before onset). Furthermore, this study adds novel longitudinal evidence by identifying an earlier divergence in the CSF Aβ42/Aβ40 ratio at 17.6 years before onset,

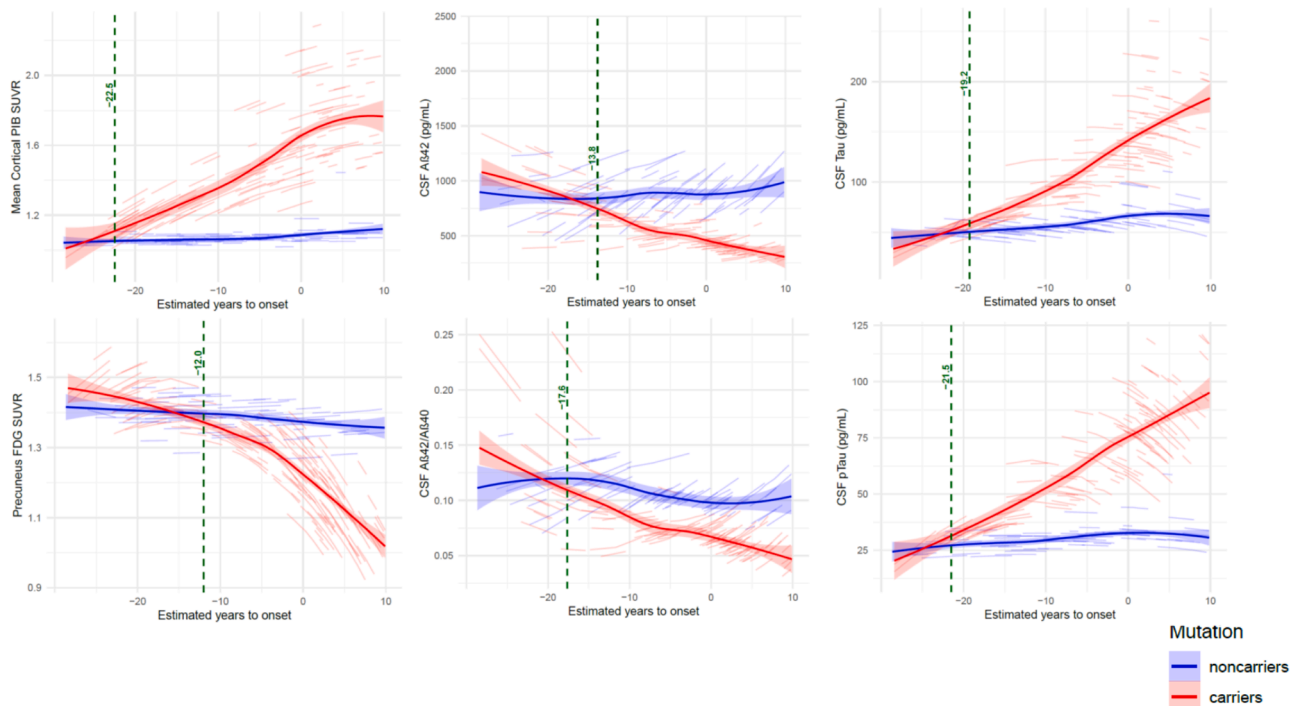


Fig. 1. Longitudinal linear mixed-effects model of the reference AD biomarkers by estimated years to symptom onset interaction with mutation status. Dotted green line and text are starting estimated years to onset point with non-overlap zone of 99% confidence interval of predicted lines for mutation carriers and non-carriers. These dotted green lines are displayed only when a significant interaction between estimated years to symptom onset and mutation status is observed.

Table 3
Longitudinal linear mixed-effects model of subcortical regional Volumes by estimated years to symptom onset interaction with mutation status.

Subcortical region		Fixed-effects coefficient	SE	df	t-value	p-value
Amygdala	Right	-6.64	2.34	346.00	-2.83	0.005
	Left	-9.18	2.09	346.00	-4.40	<0.001
Thalamus	Right	-29.79	5.03	346.00	-5.92	<0.001
	Left	-27.60	7.12	346.33	-3.88	<0.001
Putamen	Right	-24.45	5.59	346.00	-4.37	<0.001
	Left	-22.17	6.12	346.00	-3.62	<0.001
Pallidum	Right	-0.67	1.46	346.00	-0.46	0.645
	Left	-0.67	1.46	346.00	0.20	0.844
Nucleus Accumbens	Right	-3.31	0.93	346.00	-3.55	<0.001
	Left	-4.56	1.16	346.00	-3.93	<0.001
Hippocampus	Right	-26.35	4.49	346.00	-5.86	<0.001
	Left	-23.53	4.46	346.00	-5.27	<0.001
Caudate	Right	-3.18	3.69	346.00	-0.86	0.390
	Left	-2.33	3.47	346.00	-0.67	0.502

Mutation status are divided by mutation carriers and non-carriers of autosomal dominant Alzheimer's disease
* p < 0.05/14; SE = Standard Error

reinforcing the temporally ordered cascade of pathological changes.

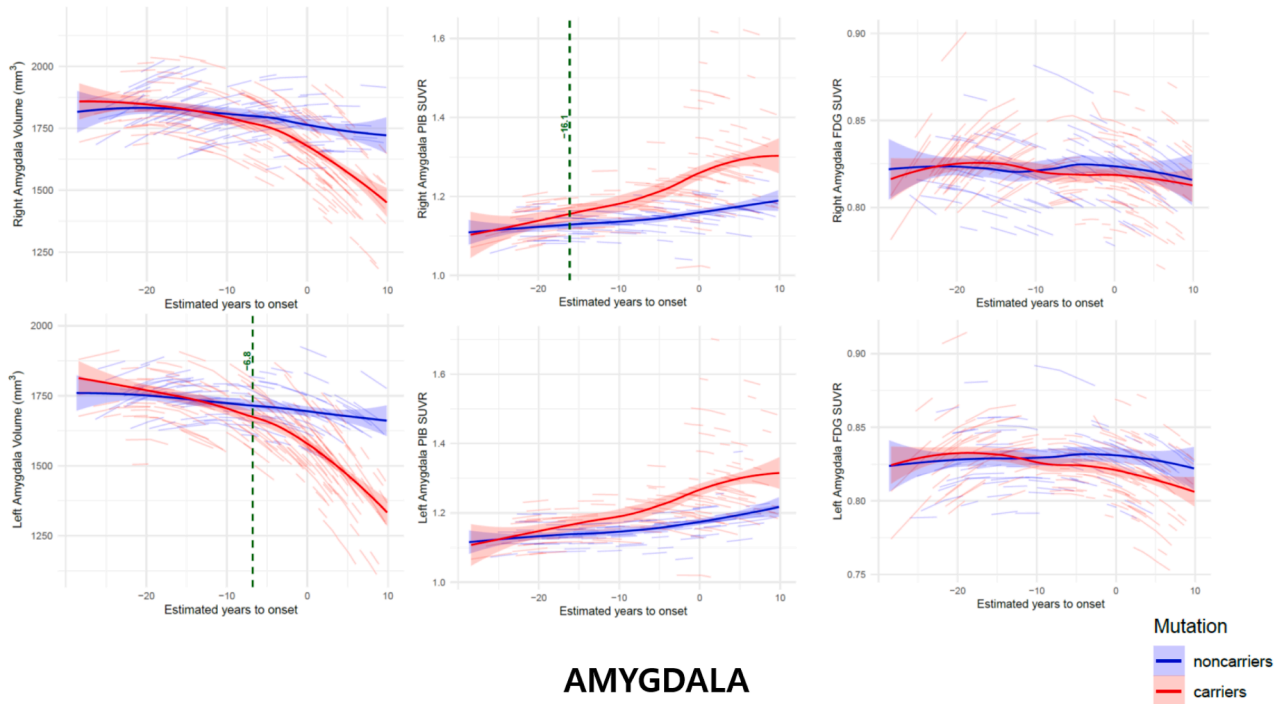
For subcortical regional analyses, we first observed that mutation carriers exhibited significantly greater longitudinal atrophy in the left amygdala, bilateral thalamus, putamen, nucleus accumbens, and hippocampus compared to non-carriers. Furthermore, carriers showed significantly higher longitudinal Aβ accumulation in most subcortical

regions, except for the left amygdala and bilateral hippocampus. Regions with significant accumulation included the right amygdala, bilateral thalamus, putamen, pallidum, nucleus accumbens, and caudate and greater hypometabolic in left hippocampus relative to non-carriers.

Among subcortical imaging biomarkers, the earliest significant difference in volume was observed in the right nucleus accumbens, occurring 13.2 years before estimated onset, followed by the left nucleus accumbens (9.5 years) and right thalamus (9.5 years). For Aβ accumulation, the right thalamus showed the earliest divergence (23.8 years before onset), followed by the left thalamus (23.2 years), and then the left nucleus accumbens and bilateral caudate (22.3 years), all of which are comparable to the timing of mean cortical Aβ deposition (22.5 years before onset). In contrast, only the left hippocampus showed a significant decline in glucose metabolism between mutation carriers and non-carriers, with divergence occurring 8.1 years before the expected symptom onset. These findings suggest a distinct temporal sequence in subcortical regions, where β-amyloidosis precedes volumetric atrophy. This pattern differs from the previously proposed temporal cascade observed in cortical regions such as the precuneus, where Aβ accumulation is followed by metabolic decline and then cortical thinning. This interpretation is supported by our region-specific second-step analyses.

In our second-step analysis, subcortical regions exhibiting significant longitudinal atrophic changes were further examined for their associations with regional Aβ accumulation and glucose metabolism. Among mutation carriers, all of these regions-except the left thalamus and bilateral hippocampus- demonstrated significant associations with region-matched Aβ accumulation. In addition, region-matched glucose metabolism was significantly associated with volume changes in the left amygdala, left thalamus, left nucleus accumbens, and bilateral hippocampus. These subcortical volumes also showed significant associations with reference AD biomarkers, including mean cortical Aβ deposition, precuneus metabolism, and CSF Tau levels in mutation carriers. When considered alongside CSF biomarker results, longitudinal atrophy of the right thalamus, bilateral putamen, and bilateral nucleus accumbens was associated with either region-specific or mean cortical Aβ accumulation,

(a)



(b)

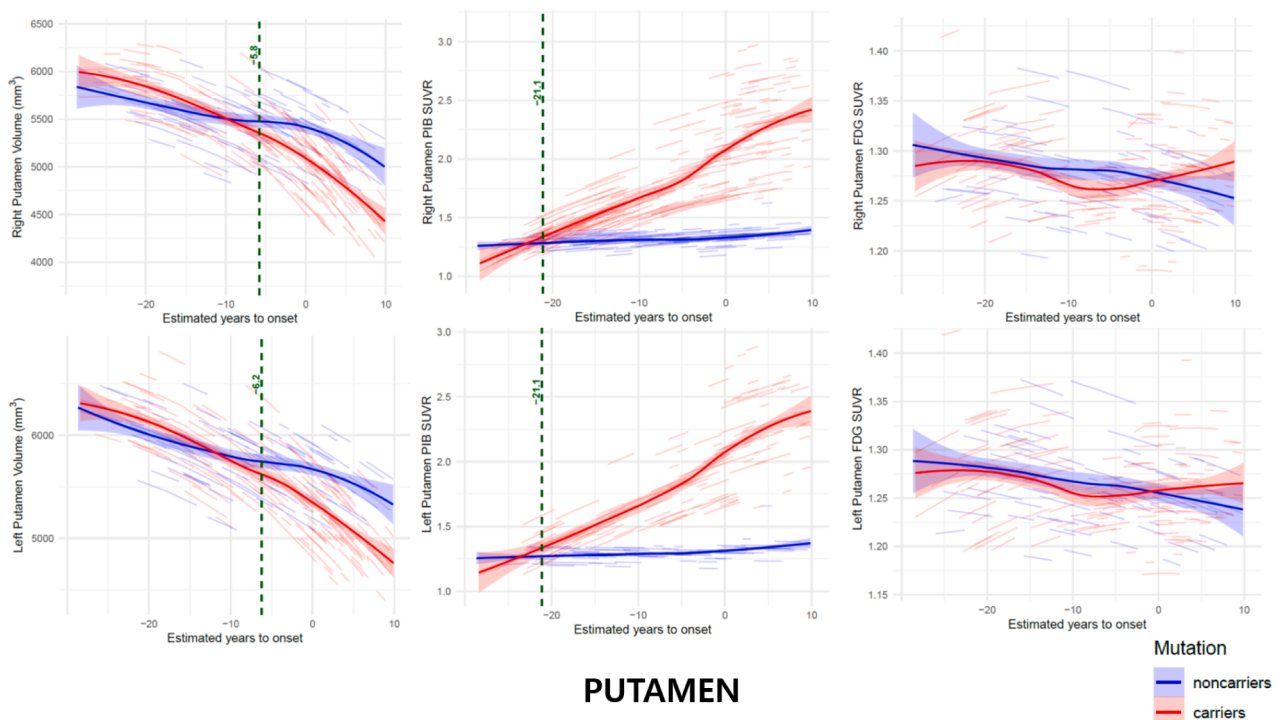
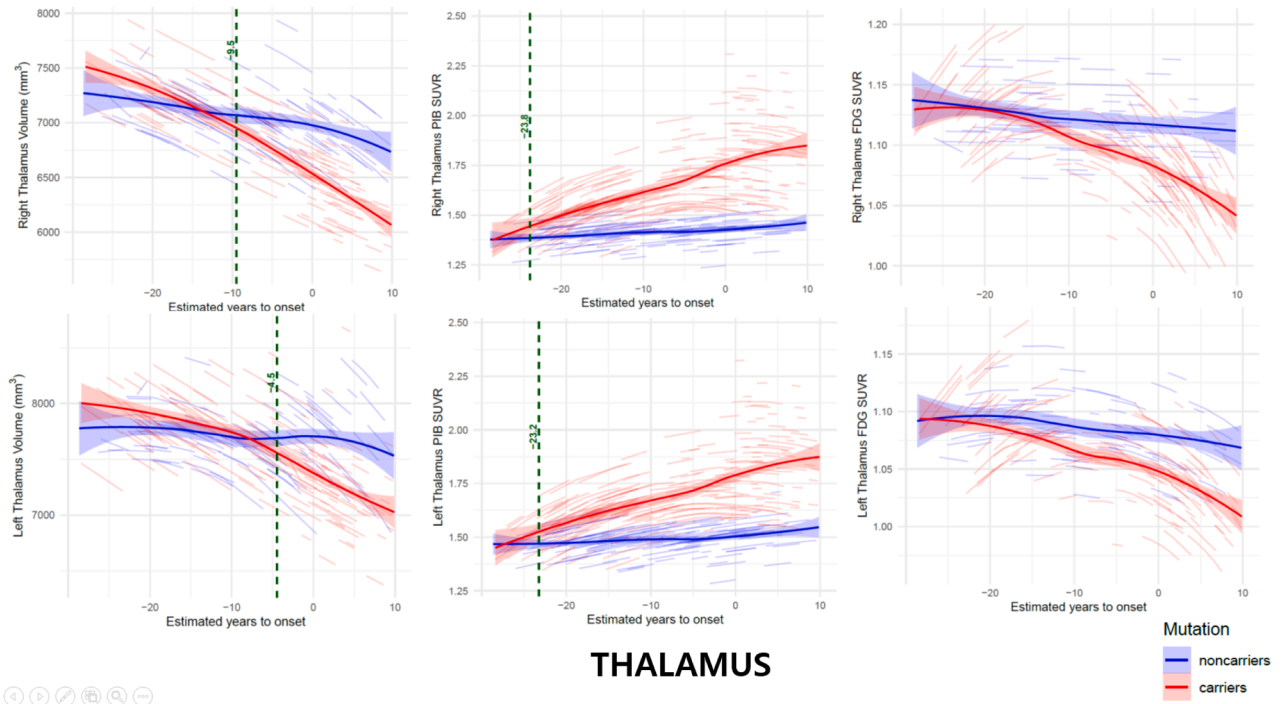


Fig. 2. Longitudinal linear mixed-effects model of the subcortical regions by estimated years to symptom onset interaction with mutation status. (a) Amygdala (b) Putamen (c) Thalamus (d) Caudate (e) Pallidum (f) Nucleus Accumbens (g) Hippocampus. Left columns are volume, middle columns are PIB SUVRs, and right columns are FDG SUVRs. The dotted green line and accompanying text indicate the estimated time point at which the 99% confidence intervals of the predicted trajectories for mutation carriers and non-carriers no longer overlap. These dotted green lines are displayed only when a significant interaction between estimated years to symptom onset and mutation status is observed. Panels that do not reach statistical significance are shown for completeness to illustrate longitudinal trajectories; interpretations in the Results and Discussion are restricted to regions and biomarkers demonstrating significant group differences.

(c)



(d)

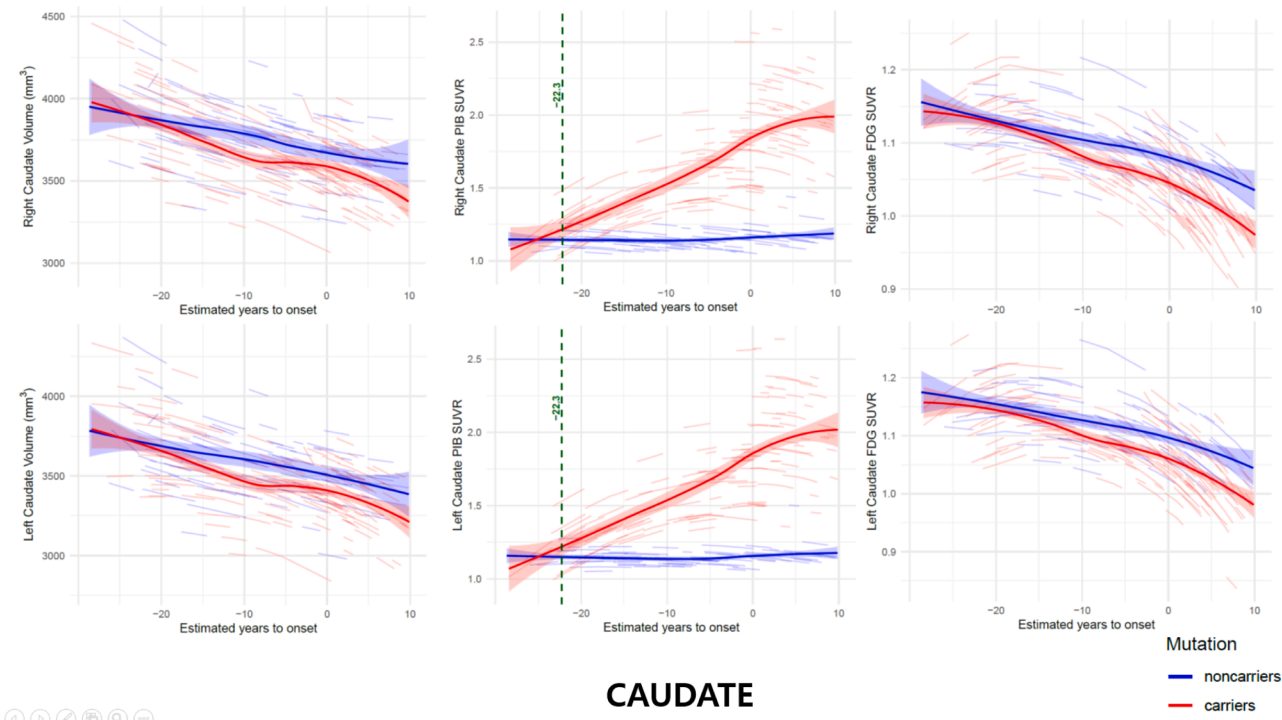


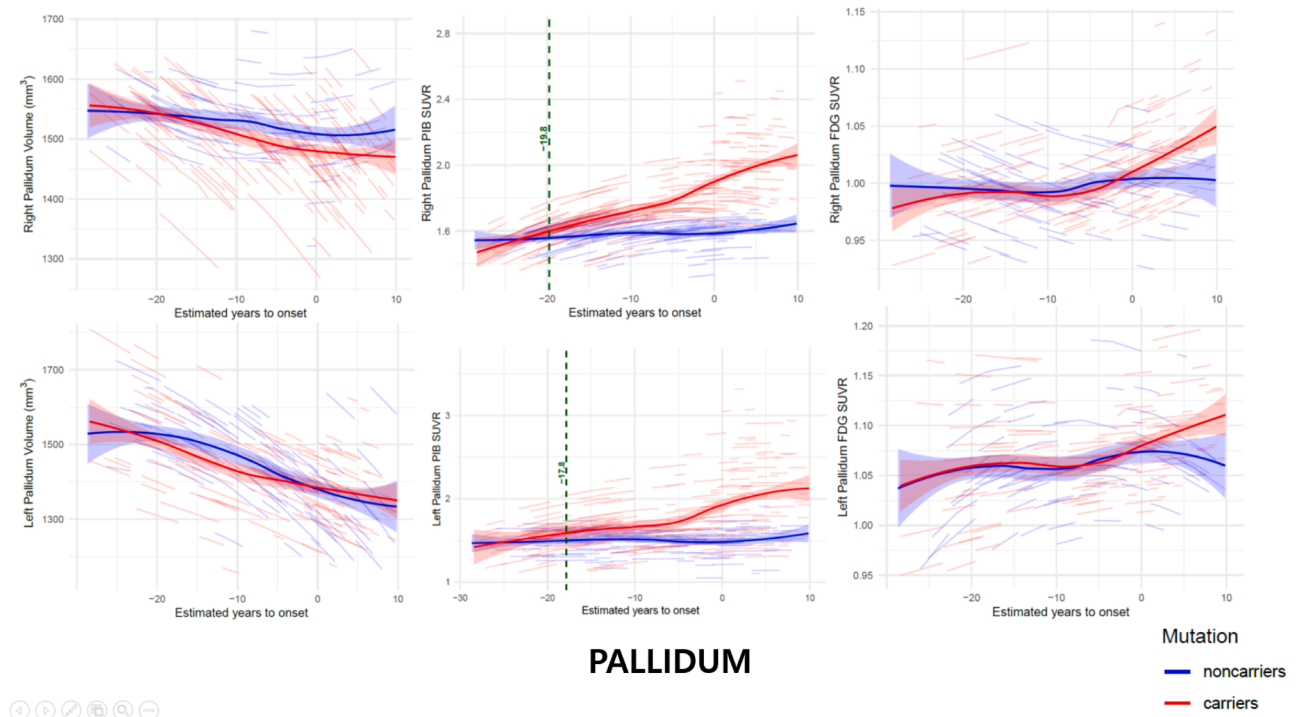
Fig. 2. (continued).

as well as with CSF A β 42, A β 42/A β 40 ratio, total Tau, and pTau. These findings suggest that longitudinal atrophy in these five subcortical ROIs reflects ongoing amyloid and tau pathophysiology in the context of dominantly inherited Alzheimer's disease. Although tau PET imaging

was not included in this study, such data could further elucidate region-specific tau pathology in these subcortical structures.

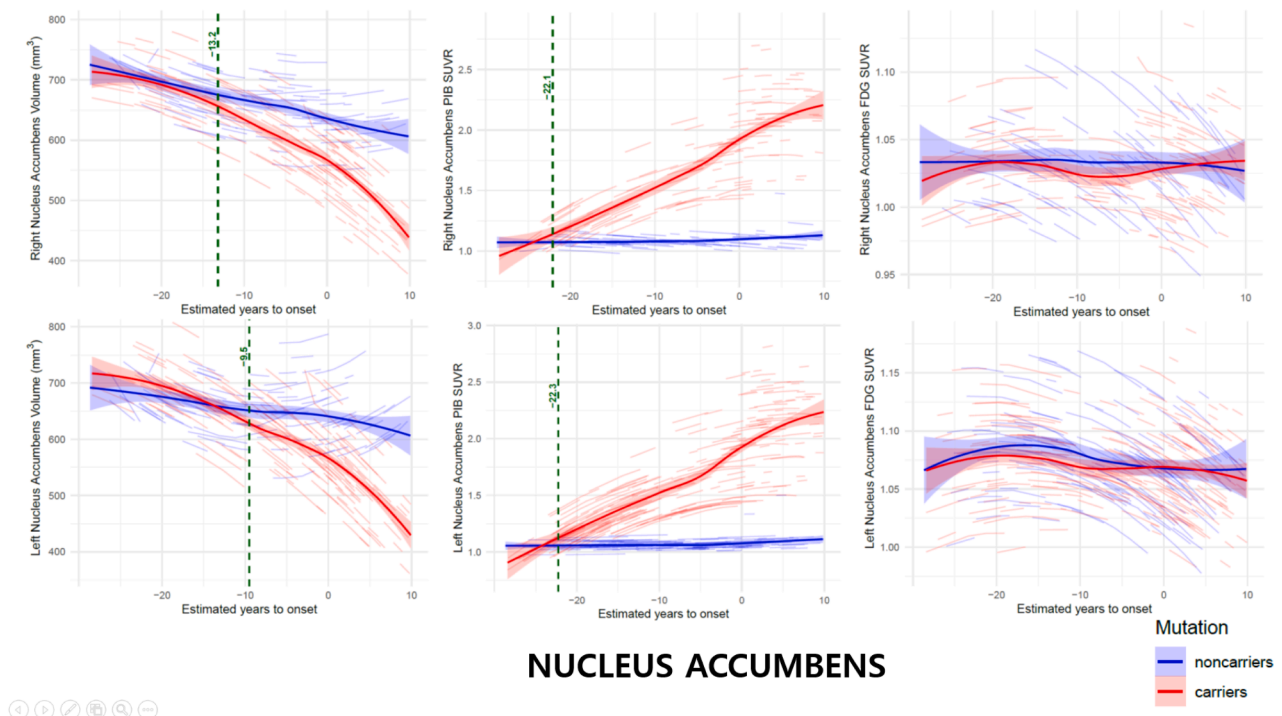
Regarding plasma biomarkers, although they had no significant interaction between mutation status and estimated years to symptom

(e)



PALLIDUM

(f)



NUCLEUS ACCUMBENS

Fig. 2. (continued).

onset, in mutation carriers plasma Aβ42 levels were associated with volumes of the right amygdala and right hippocampus. Additionally, the plasma Aβ42/Aβ40 ratio was associated with the right amygdala, right thalamus, and bilateral hippocampus. These findings suggest that

subcortical atrophy in certain regions may be related to plasma Aβ biomarker in mutation carriers.

The absence of an explicit cortical ROI analysis in the present study should be interpreted in the context of the extensive body of prior DIAN

(g)

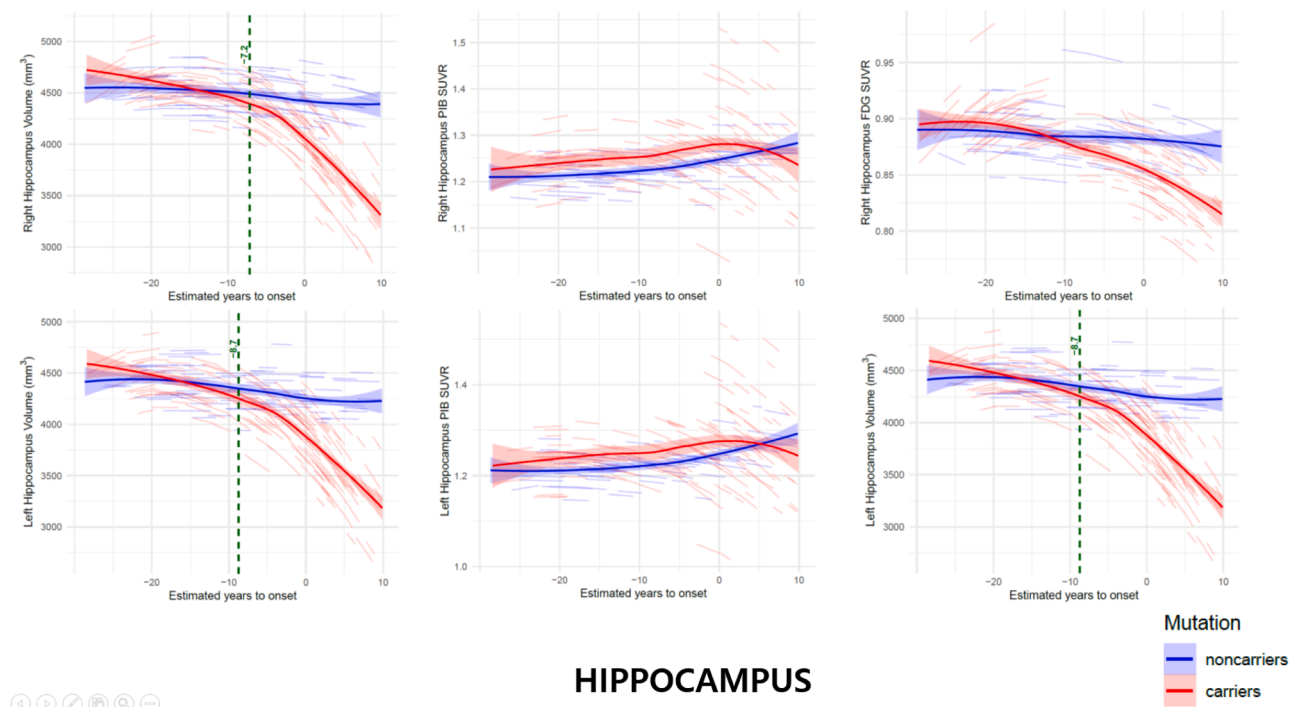


Fig. 2. (continued).

work that has already established the canonical longitudinal trajectories of cortical amyloid deposition, hypometabolism, and cortical thinning. Seminal studies have demonstrated that cortical amyloidosis begins decades before symptom onset, followed by metabolic decline and subsequent cortical atrophy, with highly consistent spatial and temporal patterns across cohorts. Given this robust and well-replicated framework, the primary objective of the current study was not to recharacterize cortical trajectories, but to address a relative gap in the literature by systematically examining subcortical regions, which have received less focused longitudinal attention despite evidence of early amyloid deposition and clinical relevance in autosomal dominant Alzheimer's disease.

Importantly, our findings suggest that subcortical biomarker trajectories may not strictly mirror the established cortical sequence. In several subcortical regions, amyloid accumulation preceded volumetric atrophy without an intermediate phase of detectable hypometabolism, contrasting with the canonical cortical cascade. By situating our results against the backdrop of prior DIAN cortical studies, we aimed to highlight these divergences rather than replicate well-established cortical effects. While direct cortical–subcortical ROI comparisons may provide additional insight, incorporating comprehensive cortical analyses would have substantially expanded the scope of the present work beyond its intended focus. Future studies explicitly designed to compare cortical and subcortical trajectories within a unified analytical framework will be important to further clarify region-specific disease propagation patterns.

The current work had a priori laterality predictions in subcortical regions, although not in the previous DIAN study [8]. The observed asymmetry in longitudinal subcortical atrophy, particularly the right-dominant involvement of the thalamus and nucleus accumbens, warrants further consideration. Asymmetric patterns of subcortical degeneration have previously been reported in sporadic Alzheimer's disease [25–27] and may reflect hemispheric differences in network connectivity, [26] vulnerability to amyloid-related pathology, [28,29]

or downstream neurodegenerative processes [30,31]. In addition, the present study incorporated a priori laterality hypotheses and leveraged longitudinal modeling, which may have enhanced sensitivity to detecting hemispheric differences over time. While the biological mechanisms underlying these asymmetries remain to be fully elucidated, our findings extend prior cross-sectional and cortical-focused observations by providing longitudinal evidence of lateralized subcortical trajectories in autosomal dominant Alzheimer's disease.

To our knowledge, the present study represents the most comprehensive and longest longitudinal analysis of biomarker data in autosomal dominant AD to date, with a specific focus on subcortical brain regions. However, the temporal sequence and relationships among biomarkers should be interpreted with caution, as individual-level data may not capture the full course of disease progression, and some individuals may deviate from the overall population trends.

Our findings suggest a distinct biomarker trajectory in subcortical regions, differing from the previously established cortical sequence of β -amyloidosis, followed by glucose hypometabolism, and subsequent structural atrophy. Specifically, β -amyloidosis appears first, and followed by subcortical volume atrophy. Moreover, subcortical volume loss is significantly associated with AD pathology. Although the present findings were derived from individuals with autosomal dominant Alzheimer's disease, this population provides a unique and well-characterized model for investigating the temporal ordering of Alzheimer's disease biomarkers. The observed sequence of early subcortical amyloid accumulation followed by volumetric atrophy may therefore inform hypotheses regarding subcortical involvement in sporadic Alzheimer's disease. However, differences in age of onset, comorbidities, and disease heterogeneity may limit direct extrapolation. Future longitudinal studies in sporadic cohorts will be necessary to determine whether similar subcortical trajectories and divergence patterns are present and to assess their potential clinical utility.

Table 4

Longitudinal linear mixed-effects model of subcortical regional PIB/FDG SUVR by estimated years to symptom onset interaction with mutation status.

Subcortical region		Fixed-effects coefficient	SE	df	t-value	p-value
PIB SUVR						
Amygdala	Right	4.322	1.1146	280.00	2.97	0.003*
	Left	4.233	1.503	280.00	2.82	0.005
Thalamus	Right	12.706	2.409	567.00	5.27	<0.001*
	Left	11.128	2.402	567.00	4.63	<0.001*
Putamen	Right	35.671	3.658	567.00	9.75	<0.001*
	Left	33.494	3.633	280.00	9.22	<0.001*
Pallidum	Right	15.234	2.700	567.00	5.64	<0.001*
	Left	20.681	3.147	280.00	6.57	<0.001*
Nucleus Accumbens	Right	35.349	3.596	280.00	9.83	<0.001*
	Left	38.048	3.628	567.00	10.46	<0.001*
Hippocampus	Right	-0.138	1.263	280.00	-0.11	0.913
	Left	-0.259	1.262	280.00	-0.21	0.838
Caudate	Right	27.894	3.485	280.00	8.00	<0.001*
	Left	28.428	3.536	280.00	8.04	<0.001*
FDG SUVR						
Amygdala	Right	-0.104	0.536	305.00	-0.19	0.847
	Left	-0.669	0.549	305.00	-1.22	0.223
Thalamus	Right	-1.167	0.717	305.00	-1.63	0.105
	Left	-1.118	0.704	305.00	-1.59	0.114
Putamen	Right	0.77	0.935	305.00	0.83	0.409
	Left	0.885	0.920	305.00	0.96	0.337
Pallidum	Right	1.908	0.795	305.00	1.38	0.169
	Left	0.615	1.090	305.00	0.56	0.573
Nucleus Accumbens	Right	-0.038	0.750	305.00	-0.05	0.959
	Left	-0.193	0.808	545.00	-0.24	0.811
Hippocampus	Right	-1.580	0.560	305.00	-2.82	0.005
	Left	-2.024	0.578	305.00	-3.50	<0.001*
Caudate	Right	-1.096	0.900	305.00	-1.22	0.224
	Left	-1.131	0.958	305.00	-1.18	0.239

Mutation status are divided by mutation carriers and non-carriers of autosomal dominant Alzheimer's disease;

* $p < 0.05/14$; SE = Standard Error; SUVR values were multiplied by 1000 for scaling

Funding

Data collection and sharing for this project was supported by The Dominantly Inherited Alzheimer Network (DIAN, UF01AG032438) funded by the National Institute on Aging (NIA), the Alzheimer's Association (SG-20-690363-DIAN), the German Center for Neurodegenerative Diseases (DZNE), Raul Carrea Institute for Neurological Research (FLENI), Partial support by the Research and Development Grants for Dementia from Japan Agency for Medical Research and Development (AMED), the Korea Health Technology R&D Project through the Korea Health Industry Development Institute (KHIDI), Korea Dementia Research Center (KDRC), funded by the Ministry of Health & Welfare and Ministry of Science and ICT, Republic of Korea RS-2024-00344521, and Spanish Institute of Health Carlos III (ISCIII). This study was supported by research fund from Chosun University (2017). Hoyoung Park was supported by the National Research Foundation of Korea (NRF) grant funded by the Korea government (MSIT) (No. RS-2023-00212502).

Declaration of the use of generative AI and AI-assisted technologies in scientific writing and in figures, images and artwork

The authors declare that generative AI and AI-assisted technologies were used solely for language editing and grammatical refinement during manuscript preparation. All scientific content, study design, data analysis, interpretation of results, and conclusions were entirely conceived and conducted by the authors.

No generative AI or AI-assisted tools were used in the creation, modification, or analysis of figures, images, or artwork.

Data statement

The data used in this study are available from the Dominantly Inherited Alzheimer Network (DIAN) upon reasonable request. Access to DIAN data requires submission of a data request application and approval by the DIAN Data Sharing Committee. Further information on data access is available at <https://dian.wustl.edu/for-investigators/>

CRedit authorship contribution statement

IL Han Choo: Writing – review & editing, Writing – original draft, Visualization, Validation, Project administration, Methodology, Funding acquisition, Formal analysis, Data curation, Conceptualization. **Hoyoung Park:** Methodology. **Brian A. Gordon:** Supervision. **Randall J. Bateman:** Validation, Supervision, Funding acquisition.

Declaration of competing interest

The authors declare that they have no known competing financial interests or personal relationships that could have appeared to influence the work reported in this paper.

Acknowledgments

This manuscript has been reviewed by DIAN Study investigators for scientific content and consistency of data interpretation with previous DIAN Study publications. We acknowledge the altruism of the participants and their families and contributions of the DIAN research and support staff at each of the participating sites for their contributions to this study.

Supplementary materials

Supplementary material associated with this article can be found, in the online version, at [doi:10.1016/j.tjpad.2026.100513](https://doi.org/10.1016/j.tjpad.2026.100513).

References

- [1] Montal V, Vilaplana E, Pegueroles J, et al. Biphasic cortical macro- and microstructural changes in autosomal dominant Alzheimer's disease. *Alzheimers Dement* 2021;17:618–28.
- [2] Millar PR, Gordon BA, Wisch JK, et al. Advanced structural brain aging in preclinical autosomal dominant Alzheimer disease. *Mol Neurodegener* 2023;18:98.
- [3] Braak H, Braak E. Neuropathological staging of Alzheimer-related changes. *Acta Neuropathol* 1991;82:239–59.
- [4] Thal DR, Rub U, Orantes M, Braak H. Phases of A beta-deposition in the human brain and its relevance for the development of AD. *Neurology* 2002;58:1791–800.
- [5] Klunk WE, Price JC, Mathis CA, et al. Amyloid deposition begins in the striatum of presenilin-1 mutation carriers from two unrelated pedigrees. *J Neurosci* 2007;27:6174–84.
- [6] Roh JH, Qiu A, Seo SW, et al. Volume reduction in subcortical regions according to severity of Alzheimer's disease. *J Neuro* 2011;258:1013–20.
- [7] Cash DM, Ridgway GR, Liang Y, et al. The pattern of atrophy in familial Alzheimer disease: volumetric MRI results from the DIAN study. *Neurology* 2013;81:1425–33.
- [8] Gordon BA, Blazey TM, Su Y, et al. Spatial patterns of neuroimaging biomarker change in individuals from families with autosomal dominant Alzheimer's disease: a longitudinal study. *Lancet Neurol* 2018;17:241–50.

- [9] McDade E, Wang G, Gordon BA, et al. Longitudinal cognitive and biomarker changes in dominantly inherited Alzheimer disease. *Neurology* 2018;91:e1295–306.
- [10] Palmqvist S, Warmenhoven N, Anastasi F, et al. Plasma phospho-tau217 for Alzheimer's disease diagnosis in primary and secondary care using a fully automated platform. *Nat Med* 2025;31:2036–43.
- [11] Morris JC. The Clinical Dementia Rating (CDR): current version and scoring rules. *Neurology* 1993;43:2412–4.
- [12] Jack Jr CR, Bernstein MA, Fox NC, et al. The Alzheimer's Disease Neuroimaging Initiative (ADNI): MRI methods. *J Magn Reson Imaging* 2008;27:685–91.
- [13] Jack Jr CR, Bernstein MA, Borowski BJ, et al. Update on the magnetic resonance imaging core of the Alzheimer's disease neuroimaging initiative. *Alzheimers Dement* 2010;6:212–20.
- [14] Fischl B. FreeSurfer. *Neuroimage* 2012;62:774–81.
- [15] Su Y, D'Angelo GM, Vlassenko AG, et al. Quantitative analysis of PiB-PET with FreeSurfer ROIs. *PLoS One* 2013;8:e73377.
- [16] Su Y, Blazey TM, Snyder AZ, et al. Partial volume correction in quantitative amyloid imaging. *Neuroimage* 2015;107:55–64.
- [17] Joshi A, Koeppe RA, Fessler JA. Reducing between scanner differences in multi-center PET studies. *Neuroimage* 2009;46:154–9.
- [18] Hajnal JV, Saeed N, Soar EJ, Oatridge A, Young IR, Bydder GM. A registration and interpolation procedure for subvoxel matching of serially acquired MR images. *J Comput Assist Tomogr* 1995;19:289–96.
- [19] Eisenstein SA, Koller JM, Piccirillo M, et al. Characterization of extrastriatal D2 in vivo specific binding of [(1)(8)F](N-methyl)benperidol using PET. *Synapse* 2012;66:770–80.
- [20] Rowland DJ, Garbow JR, Laforest R, Snyder AZ. Registration of [18F]FDG microPET and small-animal MRI. *Nucl Med Biol* 2005;32:567–72.
- [21] Shaw LM, Vanderstichele H, Knapik-Czajka M, et al. Qualification of the analytical and clinical performance of CSF biomarker analyses in ADNI. *Acta Neuropathol* 2011;121:597–609.
- [22] Shaw LM, Korecka M, Lee EB, et al. ADNI Biomarker Core: A review of progress since 2004 and future challenges. *Alzheimers Dement* 2025;21:e14264.
- [23] Bateman RJ, Xiong C, Benzinger TL, et al. Clinical and biomarker changes in dominantly inherited Alzheimer's disease. *N Engl J Med* 2012;367:795–804.
- [24] Barthelemy NR, Li Y, Joseph-Mathurin N, et al. A soluble phosphorylated tau signature links tau, amyloid and the evolution of stages of dominantly inherited Alzheimer's disease. *Nat Med* 2020;26:398–407.
- [25] Low A, Mak E, Malpetti M, et al. Asymmetrical atrophy of thalamic subnuclei in Alzheimer's disease and amyloid-positive mild cognitive impairment is associated with key clinical features. *Alzheimers Dement (Amst)* 2019;11:690–9.
- [26] Wu X, Wu Y, Geng Z, et al. Asymmetric Differences in the Gray Matter Volume and Functional Connections of the Amygdala Are Associated With Clinical Manifestations of Alzheimer's Disease. *Front Neurosci* 2020;14:602.
- [27] Kim GW, Park K, Jeong GW. Early Detection of Alzheimer's Disease in Postmenopausal Women Using Thalamic Subnuclear Volumetry. *J Clin Med* 2023;12:6844.
- [28] Kjeldsen PL, Parbo P, Hansen KV, et al. Asymmetric amyloid deposition in preclinical Alzheimer's disease: A PET study. *Aging Brain* 2022;2:100048.
- [29] Anjarv TE, Ossenkoppele R, Smith R, et al. Hemispheric asymmetry of tau pathology is related to asymmetric amyloid deposition in Alzheimer's Disease. *Nat Commun* 2025;16:8232.
- [30] Hoeng MC, Bischof GN, Seemiller J, et al. Networks of tau distribution in Alzheimer's disease. *Brain* 2018;141:568–81.
- [31] Weise CM, Chen K, Chen Y, et al. Left lateralized cerebral glucose metabolism declines in amyloid-beta positive persons with mild cognitive impairment. *Neuroimage Clin* 2018;20:286–96.